Measurement of the two-photon spectral distribution from decay of the $1s2s\ ^1S_0$ level in heliumlike nickel

H. W. Schäffer,[1] R. W. Dunford,[2,*] E. P. Kanter,[2] S. Cheng,[3] L. J. Curtis,[3] A. E. Livingston,[4] and P. H. Mokler[1]
[1]*Gesellschaft für Schwerionenforschung, D-64291 Darmstadt, Germany*
[2]*Physics Division, Argonne National Laboratory, Argonne, Illinois 60439*
[3]*Department of Physics and Astronomy, University of Toledo, Toledo, Ohio 43606*
[4]*Department of Physics, University of Notre Dame, Notre Dame, Indiana 46556*
(Received 13 July 1998)

A measurement of the shape of the spectral distribution of two-photon decay of the $1s2s\ ^1S_0$ level in heliumlike nickel is described. Uncertainties in detector efficiencies which had limited the precision of earlier measurements were eliminated by comparing the continuum emission from two-photon decays of H-like and He-like nickel. Our results are in agreement with the nonrelativistic calculation of Drake and the fully relativistic calculation of Derevianko and Johnson and suggest a method for testing relativistic atomic many-body theory in strong fields. [S1050-2947(99)05501-8]

PACS number(s): 32.70.Fw, 31.30.Jv, 31.10.+z, 32.30.Rj

I. INTRODUCTION

Two-photon decay is a second-order process in which the initial and final states of a decaying system are coupled via interactions with a complete set of intermediate states. An important example is the decay of the $1s2s\ ^1S_0$ level of helium and heliumlike ions (see Fig. 1). Due to the angular momentum selection rule (and in the absence of hyperfine effects [1]) this state is forbidden to decay to the $1s^2\ ^1S_0$ ground state by the emission of a single photon and so it decays by the simultaneous emission of two photons. A characteristic feature of this process is that the spectral distribution of the emitted photons is a broad continuum which peaks at half the transition energy. The differential transition probability has the form

$$\frac{dw_{2\gamma}}{d\omega_1}=\frac{\omega_1\omega_2}{(2\pi)^2c^2}|M_{2\gamma}|^2 d\Omega_1 d\Omega_2, \tag{1}$$

where ω_j is the energy and $d\Omega_j$ is the solid angle for the jth photon. The transition energy ω_0 satisfies energy conservation $\omega_0=\omega_1+\omega_2$. The second-order matrix element $M_{2\gamma}$ for two-photon decay of the He-like $2\ ^1S_0$ state, after summation over magnetic quantum numbers, is given by

$$M_{2\gamma}=\hat{\boldsymbol{\varepsilon}}_1\cdot\hat{\boldsymbol{\varepsilon}}_2\sum_n\left(\frac{\langle 1\ ^1S_0\|R_{E1}(\omega_2)\|n\rangle\langle n\|R_{E1}(\omega_1)\|2\ ^1S_0\rangle}{E_n-E_{2^1S_0}+\omega_1}+\frac{\langle 1\ ^1S_0\|R_{E1}(\omega_1)\|n\rangle\langle n\|R_{E1}(\omega_2)\|2\ ^1S_0\rangle}{E_n-E_{2^1S_0}+\omega_2}\right), \tag{2}$$

where $\hat{\boldsymbol{\varepsilon}}_j$ is the polarization vector for the jth photon and $R_{E1}(\omega_j)$ is the electric dipole operator.

We are making a detailed study of two-photon decay in highly charged heliumlike ions in order to test relativistic atomic many-body theories. These theories underpin our understanding of the atomic structure of few-electron heavy ions, the inner shells of heavy neutral atoms, and molecules containing these atoms. Heliumlike ions with moderate to high nuclear charge Z are the simplest systems in which both relativity and interelectron interactions are important. In attempting to understand these systems, one already encounters some nontrivial theoretical issues. For high-Z ions the relativistic expansion parameter αZ approaches one and relativistic effects must be treated exactly. Also, in a fully relativistic treatment including electron-electron interactions, eigenvalues have no lower bound due to the negative-energy states [2] and this necessitates using the no-virtual-pair approximation [3] in which the negative-energy states are left out of the calculation in lowest order. Of course, one must include the effects of the negative-energy states in higher order and their role in atomic structure is a topic of current

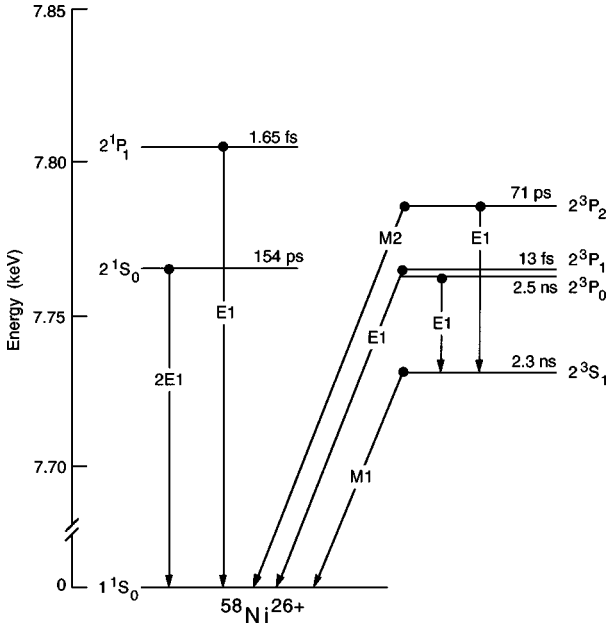

FIG. 1. Low-lying energy levels of He-like nickel showing decay modes and lifetimes.

*Author to whom correspondence should be addressed. Electronic address: dunford@anlphy.phy.anl.gov

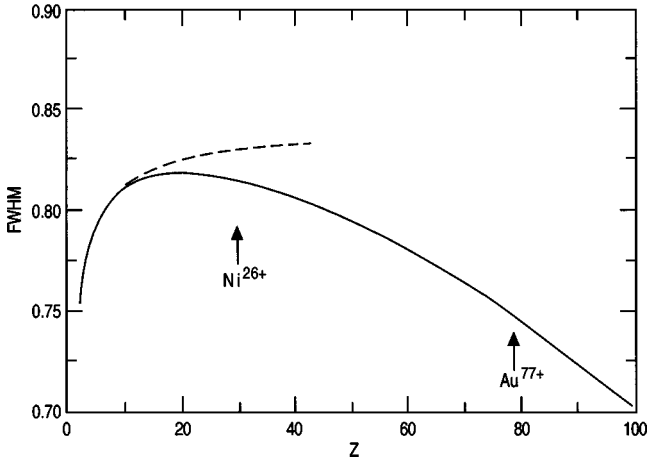

FIG. 2. Full width at half maximum (expressed as a fraction of the transition energy) of the continuum distribution for two-photon decay of He-like ions as a function of *Z*. The dotted curve is the nonrelativistic theory of Drake [14,15], while the solid curve is the fully relativistic calculation of Derevianko and Johnson [16].

interest [4,5]. Two-photon decay provides a unique way to study relativistic many-body theory because the requirement for summing over virtual intermediate states means the entire structure of the atom must be understood. Also, two-photon decay is particularly sensitive to the negative-energy states which appear explicitly in the sum over intermediate states n in Eq. (2).

In the past, studies of two-photon decay have concentrated on measurements of the lifetimes of two-photon emitting states [6]. Lifetimes of heliumlike two-photon emitters with nuclear charge (Z) ranging from $Z=2$ to $Z=41$ have been measured [7,8] with precisions as good as 1%. Good agreement with existing calculations has been found. These measurements become difficult at high Z, however, because the lifetime of the $1s2s\ ^1S_0$ state becomes too short to measure accurately with existing techniques. In order to surmount this problem, we have undertaken a study of the spectral distributions of the continua from two-photon decay. Apart from the trivial factor $\omega_1\omega_2$ [see Eq. (1)], measurement of the spectral distribution determines the energy dependence of the square of the second-order matrix element $M_{2\gamma}$ given by Eq. (2). The advantage is that these measurements can be made for any He-like ion, and they provide information far beyond what can be learned from lifetime measurements which determine the transition probabilities summed over the spectral distributions.

In the nonrelativistic theory, the shape of the spectral distribution for two-photon decay of the $2\ ^2S_{1/2}$ level in one-electron ions is independent of Z [9,10], but in a fully relativistic treatment the distribution becomes narrower as Z increases [11–13]. By contrast, in He-like ions, the nonrelativistic calculations predict an increase in the width of the distribution as Z is increased [14,15] as indicated by the dashed curve in Fig. 2. The recent fully relativistic calculation of the two-photon decay rate for the $2\ ^1S_0$ level in heliumlike ions by Derevianko and Johnson [16] shows a more complicated dependence (solid line in Fig. 2). At low Z the width follows that of the nonrelativistic calculation, increasing with Z, whereas at high Z the distribution narrows. In order to test these predictions, we are pursuing a program which includes a precision measurement of the continuum spectrum at intermediate Z, near the maximum width, and another measurement at high Z where a significant narrowing is expected. In this paper we report the results of an experiment utilizing heliumlike nickel ($Z=28$) which accomplishes the first part of this program. The second part will involve measuring the spectral distribution from decay of the $2\ ^1S_0$ state in heliumlike gold ($Z=79$) being done [17,18] at the heavy ion synchrotron in Darmstadt, Germany.

II. BACKGROUND

In the late 1960s Elton, Palumbo, and Griem [19] studied the continuum emission from He-like Ne in a plasma discharge, using a grazing incidence spectrometer, and made a rough verification of the spectral distribution of two-photon decay. In other early work, Artura, Tolk, and Novick [20] used broadband filters to study the continuum emission from the decay of the $2\ ^2S_{1/2}$ level in a beam of singly ionized helium, and O'Connell *et al.* [21] made similar measurements using hydrogen. Also, Schmieder and Marrus [22] observed the continuum radiation from the two-photon decay of metastable states in H-like and He-like argon using beam-foil spectroscopy and solid state Si(Li) detectors.

We recently completed a detailed study of the continuum shape for two-photon decay in He-like krypton [23]. This experiment involved observing coincidences between pairs of Si(Li) detectors whose efficiencies as a function of photon energy had been measured over a broad range (1–15 keV). The comparison between theory and experiment was done with the aid of a Monte Carlo simulation. Although the results were in agreement with the nonrelativistic calculations of Drake, the errors in the simulation due to uncertainties in detector efficiencies were on the order of the difference in the theoretical shapes between helium ($Z=2$) and He-like Kr ($Z=36$) and this measurement was not of sufficient precision to provide the needed determination of the spectral shape for intermediate-Z ions. Because it appeared difficult to significantly improve our determination of the efficiency of the Si(Li) detectors particularly in the region below 3 keV, a new experimental approach was needed.

In the present experiment we were able to overcome the former limitations by measuring two-photon decay in both hydrogenlike and heliumlike nickel in the same experiment, switching between the two ions several times during the measurement. Since the continuum shape in the two-photon decay of the $^2S_{1/2}$ level in H-like Ni is known precisely, this served as a calibration of the spectral efficiency of the detection system.

III. EXPERIMENT

A detailed description of the experimental apparatus used in this experiment is given in Ref. [23] so only a brief discussion will be given here. A beam of 11.7-MeV/u ^{58}Ni ions from the Argonne Tandem Linear Accelerator System (ATLAS) was stripped in a 200-μg/cm^2 C foil and alternately the 26+ and 28+ charge states were directed to our target chamber by a bending magnet. That foil was located at

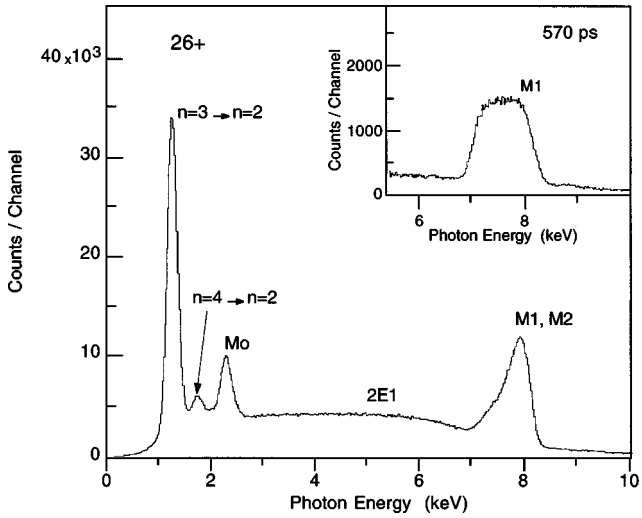

FIG. 3. Singles spectrum from detector A with Ni^{26+} incident on a 10 $\mu g/cm^2$ carbon target. The detector was shielded from a direct view of the foil. The inset shows a spectrum taken with the foil moved upstream so that the flight time to the detectors was 570 ps.

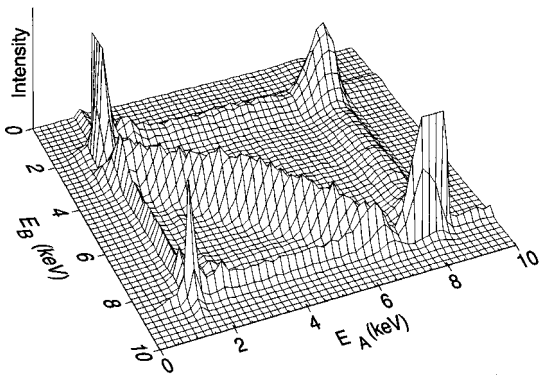

FIG. 4. Coincidence intensity as a function of the energies E_A and E_B deposited in detectors A and B with Ni^{28+} incident on target.

a beam focus midway between the end of ATLAS and the bending magnet. This arrangement minimized the degradation of the beam emittance caused by straggling in the foil. A time-of-flight beam energy measuring system, also located in this region, determined the beam velocity to better than 1%. This information was needed for Monte Carlo simulations of the experiment. A 2-mm-diam removable aperture located just upstream of the target chamber was used during beam focusing and about 80% of the beam could be transmitted through this aperture at best focus. The aperture was removed during data taking but it was periodically reinserted to check the position and focus of the beam which were found to be stable on the time scale of about a day. The aperture also allowed us to precisely reproduce the beam conditions after changing the charge state.

In the target chamber, the beam was excited in a thin C foil (10 $\mu g/cm^2$) and x rays from the decay of the excited states were studied using an array of three Si(Li) detectors which measured x rays emitted perpendicular to the beam. A molybdenum shield was used to block the intense x rays from short-lived states formed at the foil. A typical spectrum recorded with one of the Si(Li) detectors for Ni^{26+} incident on target is given in Fig. 3. The peak just below 8 keV is a blend of lines from decays of the $2\,^3S_1$ and $2\,^3P_2$ levels in He-like nickel. The asymmetric line shape arises from an interplay between the spread in Doppler shifts due to the finite observation angle and the lifetimes of the states (see Fig. 1). First consider the inset to Fig. 3 which was taken with the foil moved upstream from the normal position so that the shorter-lived $2\,^3P_2$ state has decayed away before the ions reach the field of view of the detectors. In this case, only the long-lived $2\,^3S_1$ state (decay length $\sim$11 cm) contributes and there is considerable broadening due to the extended source length. With the foil in the normal position, there is an additional contribution from the $2\,^3P_2$ state which is narrower due to the smaller source size (decay length $\sim$3.4 mm) and shifted to higher energy because the source is located upstream from the center of the detector field of view. The line shapes for both the upstream and normal position have been precisely modeled by a Monte Carlo simulation of the experiment.

At the low-energy end of the spectrum, contributions from decays into $n=2$ from higher-lying levels of He-like, Li-like, or lower charge state ions appear together with a line arising from fluorescence of the target shield and detector masks which are made of molybdenum. Two-photon decay contributes to the continuum in the center of the plot. Due to the line structures, and because there are other contributions to the continuum region, it is not possible to determine the shape of the continuum from the singles spectrum and we must rely on coincidence techniques to unambiguously identify the two-photon decays.

Figure 4 shows the matrix of coincidence events as a function of the energies E_A and E_B recorded in detector A and detector B with Ni^{28+} incident on target. The events corresponding to two-photon decay of H-like nickel appear as a diagonal ridge at a constant sum energy. The four (corner) peaks are due to coincidences between single-photon lines. These can be accidental coincidences or true coincidences arising from cascades. The ridges parallel to the axes are coincidences between single-photon lines and the continuum. Some of these are true coincidences from cascade feeding of the $2\,^1S_0$ level. Although the diagonal ridge provides a unique signature for the two-photon decays, ambiguities appear in regions where the diagonal ridge overlaps the other ridges. In order to study these regions of the plot, it is useful to consider a different view of the same data shown in Fig. 5 which is a matrix of coincidence events as a function of the sum energy and the energy E_A deposited in detector A. In this picture the two-photon events all lie along a ridge of constant sum energy. The unwanted events can be eliminated by studying projections from this matrix onto the sum-energy axis. Examples of such projections are shown in Figs. 6 and 7. Notice that the sum-energy lines maintain a fixed position while unwanted events appear as a background under the peak or as peaks which move to the right as the energy E_A increases. In either case the true two-photon events corresponding to a given E_A can be picked out by a peak fitting procedure.

An important requirement in this experiment was the ability to separate the He-like two-photon decays from the H-like two-photon decays. This was accomplished by fitting the sum-energy spectra to two peaks separated by the 308-eV

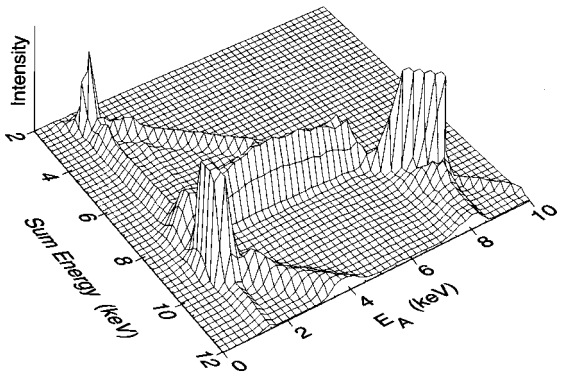

FIG. 5. Detector-A–detector-B coincidence intensity as a function of the sum energy and the energy in detector A (E_A) for the same data sample shown in Fig. 4.

energy difference between the transition energies in H-like and He-like nickel. This fitting required some care since the full width at half maximum (FWHM) of the (Doppler broadened) sum-energy lines was about 600 eV. In order to gain a detailed understanding of the shapes of the sum-energy lines, we first determined the resolutions of the Si(Li) detectors as a function of energy using radioactive sources. These data were put into the Monte Carlo simulation [23] of our experiment together with information on the geometry and efficiencies of the detectors, the ion beam velocity and spatial distribution, and the lifetimes and transition energies of the states involved. The simulation program was checked by comparing the data with the predictions for the line shapes of the single-photon lines and excellent agreement was obtained. The simulation provided us with digital representations of the exact line shapes which were used in a multiple-linear-regression routine to determine the composition of the sum-energy lines. The results of the fitting procedure indicated that with Ni^{26+} on target, the two-photon decays were mostly from decay of the $1s2s\ ^1S_0$ state of heliumlike nickel with $(3\pm2\%)$ from the H-like $2\ ^2S_{1/2}$ level. With Ni^{28+} on

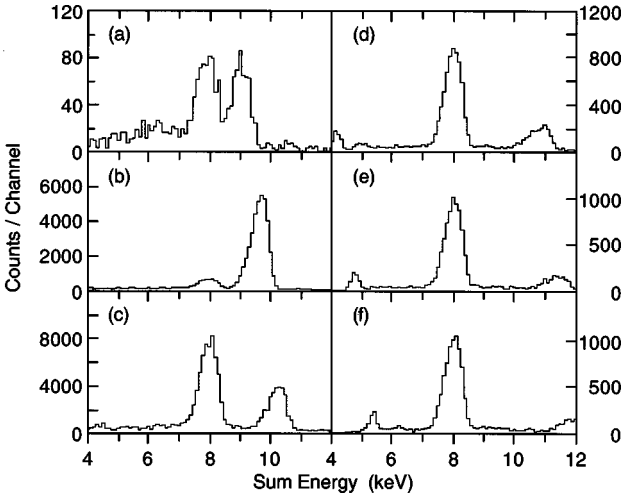

FIG. 6. Data taken with Ni^{28+} ions incident on a 10 μg/cm^2 carbon target. Sum-energy spectra for detector-A–detector-B coincidences with a condition that E_A lies within a 200-eV window centered at (a) 0.9 keV, (b) 1.5 keV, (c) 2.1 keV, (d) 2.7 keV, (e) 3.3 keV, and (f) 3.9 keV.

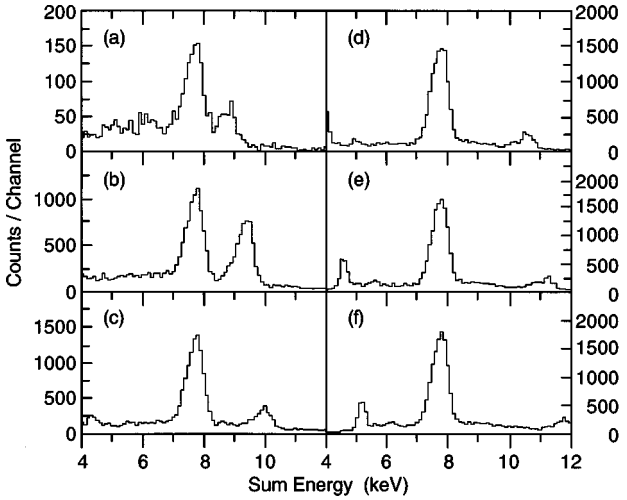

FIG. 7. Same as Fig. 6 but with Ni^{26+} incident on target.

target most of the two-photon decays were from the H-like $2\ ^2S_{1/2}$ level, but there was a $(2\pm2\%)$ contamination from the He-like $2\ ^1S_0$ state.

Other two-photon emitters that could contribute to our data include the $2\ ^3S_1$ and $2\ ^3P_0$ levels in He-like ions. Two-photon decay of the $2\ ^3S_1$ level has a spectral distribution that is markedly different than that for the $2\ ^1S_0$ level. It is zero at the midpoint of the distribution and peaks near either end point [16,24–27]. This state will not contribute significantly to our results for two reasons. First, the state decays mostly to the ground state via an $M1$ transition and has only a 0.046% branch for two-photon decay [16]. Second, because of the much longer lifetime of the $2\ ^3S_1$ state (2.3 ns) [16] compared to that of the $2\ ^1S_0$ level (154 ps) [28], most of the decays occur out of view of the detector. The $2\ ^3P_0$ level is even less likely to contribute to our results since it decays predominantly to the $2\ ^3S_1$ state with only a 0.001% branch to decay via two-photon decay [29]. It also has a long lifetime (2.5 ns) and so it also has only a small probability to decay within view of the detectors.

IV. RESULTS AND DISCUSSION

The procedure for extracting the two-photon spectral distribution from the coincidence data was similar to that used in our Kr^{34+} measurement and is described in detail in Ref. [23]. For each data set, we analyzed sum-energy spectra corresponding to 200-eV wide cuts on energy in detector A or detector B (see Figs. 6 and 7). We fit the sum-energy peaks in these spectra to determine the two-photon intensity as a function of energy. Figure 8 shows typical results. We took advantage of the symmetry of the spectral distributions about the midpoints to improve the statistical accuracy, combining the results from detectors A and B for the lower half of the distribution. The data were compared with the results of the Monte Carlo simulation and satisfactory agreement with the theoretical calculations was obtained although, as in our earlier Kr^{34+} measurement, there were large uncertainties in the Monte Carlo results.

To improve our results for He-like nickel, we used the data for hydrogenlike nickel together with the well-known theory for one-electron ions to provide a mapping function

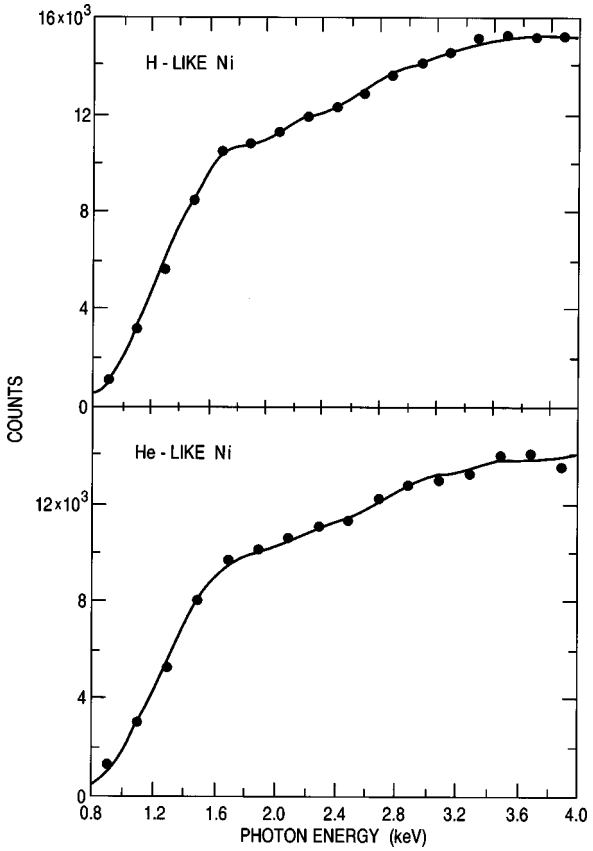

FIG. 8. Raw two-photon continuum distributions for Ni^{28+} ions incident on the target (upper graph) and for Ni^{26+} ions on target (lower graph). Solid lines are the result of Monte Carlo simulations for H-like and He-like ions.

used to deconvolve the spectral shape. The measured energy spectrum $N(E)$ is related to the underlying spectral shape $S(f)$ by a convolution integral

$$N(E)=\int_0^1 G(E,f\varepsilon)S(f)df, \tag{3}$$

where f is the fraction of the transition energy (ε) carried by the photon in the frame of the atom and E is the response of the detector system to that photon. The convolution function $G(E,f\varepsilon)$ has previously been evaluated by a Monte Carlo procedure. In this measurement we have taken advantage of the fact that the function G, as determined by simulation, is approximately symmetric in $f\varepsilon$ and sufficiently narrow in comparison to our histogram bins (200 eV) that it can be approximated by

$$G'(E)=G(E,f\varepsilon)\,\delta(E-f\varepsilon) \tag{4}$$

and hence

$$N(E)\simeq G'(E)S(E/\varepsilon). \tag{5}$$

The accuracy of this method was tested through Monte Carlo simulation and it was demonstrated that the spectral shape deconvolved by this procedure agreed over the entire range with the input distribution to $\leqslant 1\%$.

Two different methods were used to determine the mapping function $G'(E)$ from the H-like data. In the first method

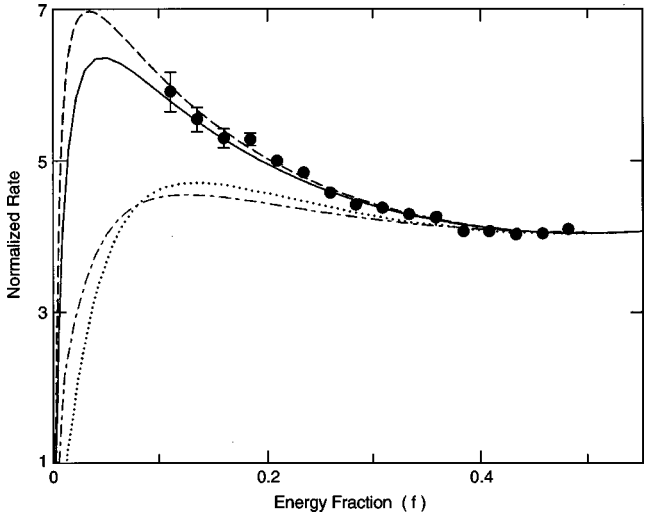

FIG. 9. Rate for two-photon decay as a function of the photon energy (in units of the fraction of the transition energy). The data for He-like nickel are compared with Drake's (dashed curve) and Derevianko and Johnson's (solid line) calculations. Also shown are Derevianko and Johnson's predictions for $Z=2$ (dotted line), and $Z=79$ (dot-dashed line). All data are normalized to the area under the last four data points. The data and theory have been divided by a factor $f(1-f)$.

$G'(E)$ was simply defined as the ratio of the H-like experimental intensity to $S(E/\varepsilon)$ using Drake's spectral shape for H-like Ni.

The second method takes into account that, as a result of small differences in the lifetimes of the H- and He-like states, the mapping function for H-like nickel $G'_{\mathrm{H}}(E)$ is slightly different from the mapping function for He-like nickel $G'_{\mathrm{He}}(E)$. The function $G'_{\mathrm{H}}(E)$ is obtained as in method I. To obtain $G'_{\mathrm{He}}(E)$, the Monte Carlo simulation was run for H-like ions and He-like ions but assuming a uniform distribution of photons from $E=0$ to $E=E_0$. This gives Monte Carlo generated mapping functions $G'^{\mathrm{MC}}_{\mathrm{H}}(E)$ and $G'^{\mathrm{MC}}_{\mathrm{He}}(E)$. Then by comparing the Monte Carlo generated mapping fuction $G'^{\mathrm{MC}}_{\mathrm{H}}(E)$ with the method I mapping function $G'_{\mathrm{H}}(E)$ for H-like nickel, we determine an energy-dependent correction to the simulated $G'^{\mathrm{MC}}_{\mathrm{H}}(E)$. We then apply the same correction to $G'^{\mathrm{MC}}_{\mathrm{He}}(E)$ to obtain $G'_{\mathrm{He}}(E)$.

The deconvoluted distributions were input to the simulation and the resulting spectra compared to the data (see Fig. 8) to verify the quality of the deconvolution procedure. The spectral shapes produced by these two methods were in excellent agreement. We have adopted the latter method for the results presented here.

The determination of the mapping function $G'_{\mathrm{He}}(E)$ enabled us to obtain a model-independent determination of the underlying shape of the two-photon distribution in He-like nickel. The results are shown in Fig. 9, which is a plot of the He-like spectral distribution vs the photon energy (f) in units of the transition energy. These data have been normalized by dividing by $f(1-f)$, representing the product $\omega_1\omega_2$ of the two photon energies, so they are proportional to the square of the second-order matrix element $M_{2\gamma}$ up to a multiplicative constant [see Eq. (1)]. Again, we exploit the symmetry of these curves about the midpoint of the distribution and show

only the low-energy half combining data for detectors *A* and *B*. The data are given by the solid dots with error bars. The solid line is the theoretical distribution of Derevianko and Johnson [16] and the dashed line is the nonrelativistic result of Drake [14,15]. The dot-dashed line is the relativistic result for Au ($Z=79$) and the dotted line is the same for He ($Z=2$).

The most interesting feature of the theoretical curves is the qualitative difference between the shape for He-like nickel, which has a prominent peak at low energy, and that for He-like Au, which is flatter. The data clearly follow the expected shape for intermediate *Z*, confirming both the relativistic calculations of Derevianko and Johnson [16] and Drake's nonrelativistic calculations [14,15] for nickel. At the lowest energy for which we have data the experimental curve differs from the calculation for He-like Au by ten standard deviations. More importantly, the data show the expected qualitative shape with a significant rise towards low energy.

The results given in Fig. 9, which are based on comparison between spectra from H-like and He-like nickel, are a marked improvement over our previous measurement of the shape of the continuum radiation from the $2\,^1S_0$ state in He-like Kr. They demonstrate that measurements of two-photon continua provide a viable means for testing theoretical calculations of two-photon transition probabilities. For future work, it is desirable to obtain sensitivity to the relativistic corrections at intermediate *Z*. The form of the theoretical curves in Fig. 9 suggests that the best approach is to extend the data to lower energy where the relativistic effects are larger. In order to do this we need to improve the coincidence detection efficiency at low energy and this is a nontrivial challenge. Sensitivity below 1 keV could be improved by using windowless Si(Li) detectors, but the more difficult problem is the poor time resolution at low energy.

Another approach to testing relativistic corrections to He-like two-photon decay is to compare our nickel results with a measurement of the spectral shape of two-photon decay at high *Z* such as in He-like gold ($Z=79$) where the relativistic corrections are more important. As indicated in Fig. 9, the shape of the two-photon distribution in Au is qualitatively different from the shape for He-like nickel and our data are sensitive to this difference.

ACKNOWLEDGMENTS

We are indebted to B. J. Zabransky and C. Kurtz, and to the staff of ATLAS for excellent technical assistance during this experiment. We thank W. R. Johnson, H. G. Berry, Th. Stöhlker, and G. W. F. Drake for stimulating discussions. This work was supported by the U.S. Department of Energy, Office of Basic Energy Sciences, Division of Chemical Sciences, and by a NATO travel grant.

[1] V. V. Karasiev, L. N. Labzowsky, and A. V. Nefiodov, Phys. Lett. A **172**, 62 (1992).
[2] G. E. Brown and D. G. Ravenhall, Proc. R. Soc. London, Ser. A **208**, 552 (1951).
[3] J. Sucher, Phys. Rev. A **22**, 348 (1980).
[4] P. Indelicato, Phys. Rev. Lett. **77**, 3323 (1996).
[5] W. R. Johnson, D. R. Plante, and J. Sapirstein, in *Advances in Atomic, Molecular and Optical Physics*, edited by B. Bederson and H. Walther (Academic Press, San Diego, 1995), Vol. 35, p. 255.
[6] R. Marrus and P. J. Mohr, Adv. At. Mol. Phys. **14**, 181 (1978).
[7] R. W. Dunford, H. G. Berry, D. A. Church, M. Hass, C. J. Liu, M. L. A. Raphaelian, B. J. Zabransky, L. J. Curtis, and A. E. Livingston, Phys. Rev. A **48**, 2729 (1993).
[8] A. Simionovici, B. B. Birkett, J. P. Briand, P. Charles, D. D. Dietrich, K. Finlayson, P. Indelicato, D. Liesen, and R. Marrus, Phys. Rev. A **48**, 1695 (1993).
[9] S. Klarsfeld, Phys. Lett. **30A**, 382 (1969).
[10] S. Klarsfeld, Lett. Nuovo Cimento **1**, 682 (1969).
[11] S. P. Goldman and G. W. F. Drake, Phys. Rev. A **24**, 183 (1981).
[12] W. R. Johnson, Phys. Rev. Lett. **29**, 1123 (1972).
[13] F. A. Parpia and W. R. Johnson, Phys. Rev. A **26**, 1142 (1982).
[14] G. W. F. Drake, Phys. Rev. A **34**, 2871 (1986).
[15] G. W. F. Drake, University of Windsor, report, 1988 (unpublished).
[16] A. Derevianko and W. R. Johnson, Phys. Rev. A **56**, 1288 (1997).
[17] H. W. Schäffer *et al.*, GSI Scientific Report No. GSI 98-1, 1998.
[18] H. W. Schäffer *et al.*, Nucl. Instrum. Methods B Phys. Res. (to be published).
[19] R. C. Elton, L. J. Palumbo, and H. R. Griem, Phys. Rev. Lett. **20**, 783 (1968).
[20] C. J. Artura, N. Tolk, and R. Novick, Astrophys. J. **157**, L181 (1969).
[21] D. O'Connell, K. J. Kollath, A. J. Duncan, and H. Kleinpoppen, J. Phys. B **8**, L214 (1975).
[22] R. W. Schmieder and R. Marrus, Phys. Rev. Lett. **25**, 1692 (1970).
[23] R. Ali, I. Ahmad, R. W. Dunford, D. S. Gemmell, M. Jung, E. P. Kanter, P. H. Mokler, H. G. Berry, A. E. Livingston, S. Cheng, and L. J. Curtis, Phys. Rev. A **55**, 994 (1997).
[24] O. Bely and P. Faucher, Astron. Astrophys. **1**, 37 (1969).
[25] O. Bely, J. Phys. B **1**, 718 (1968).
[26] G. W. F. Drake and A. Dalgarno, Astrophys. J. **152**, L121 (1968).
[27] G. W. F. Drake, G. A. Victor, and A. Dalgarno, Phys. Rev. **180**, 25 (1969).
[28] R. W. Dunford, M. Hass, E. Bakke, H. G. Berry, C. J. Liu, M. L. A. Raphaelian, and L. J. Curtis, Phys. Rev. Lett. **62**, 2809 (1989).
[29] Our own calculation using the method outlined in G. W. F. Drake, Nucl. Instrum. Methods Phys. Res. B **9**, 465 (1985).